# Novel Biocompatible Trianglamine Networks for Efficient Iodine Capture

Belkacem Tarek Benkhaled, Arnaud Chaix, Chaimaa Gomri, Sébastien Buys, Nabil Namar, Nadine Sehoulia, Rohitkumar Jadhav, Jason Richard, Laure Lichon, Christophe Nguyen, et al.

# Novel Biocompatible Trianglamine Networks for Efficient Iodine Capture

Belkacem Tarek Benkhaled,[§‡] Arnaud Chaix,*[§‡] Chaimaa Gomri,[‡] Sébastien Buys,[‡] Nabil Namar,[‡] Nadine Sehoulia,[‡] Rohitkumar Jadhav,[‡] Jason Richard,[‡] Laure Lichon,[†] Christophe Nguyen,[†] Magali Gary-Bobo,[†] and Mona Semsarilar*[‡]

[‡] Institut Européen des Membranes, IEM, Univ Montpellier, CNRS, ENSCM, Montpellier, France.

[†] Institut des Biomolécules Max Mousseron, IBMM, Univ Montpellier, CNRS, ENSCM, Montpellier, France.

***KEYWORDS. Trianglamine, Polymer Network, Adsorption, Iodine Capture, and Iodine recovery.***

**ABSTRACT:** Herein, we report for the first time a biocompatible crosslinked trianglamine (Δ) network for the efficient iodine removal from vapor phase, water and seawater. In vapor phase, the crosslinked network could capture 6 g $g^{-1}$ of iodine, ranking among the most performant materials for iodine vapor capture. In liquid phase, this crosslinked network is also capable of capturing iodine at high rates from aqueous media (water and seawater). This network displayed fast adsorption kinetics and they are fully recyclable. This study reveals the high affinity of iodine with the intrinsic cavity of the trianglamine. The synthesized material are extremely interesting since they are environmentally friendly, inexpensive and the synthesis could easily be scaled up to be used as the material of choice in response to accidents in nuclear industry.

## INTRODUCTION

Nuclear energy provides about 10% of the world's electricity production (~ 413 GW nowadays) and it is foreseen to increase, given the global circumstances. Nuclear energy plays a crucial role since it effectively responds to major global challenges such as greenhouse gas emissions, growing demand for electricity, and the need to have self-sufficient national energy sources. The International Energy Agency (IEA) predicts about $1.1 trillion in investment in nuclear plants by 2040, representing a 46% increase in nuclear power generation worldwide.[1] Due to this policy, it is urgent to come up with innovative, effective, and low-cost solutions to prevent nuclear waste pollution risks. Nuclear power plant accidents are responsible for massive radionuclide environmental contamination. Nuclear waste substances, such as radioactive iodine produced from uranium fission, release volatile solid gases and can easily dissolve in water, posing serious threats to human population as well as the ecosystem. In this circumstance, it is vital to design smart materials able to capture radioactive iodine from vapor phase, water and seawater. Radioiodine such as $^{131}I$ and $^{129}I$ are the two main components of nuclear waste, with half-lives of 8.02 days and 15.7 million years, respectively.[2] The waste streams of nuclear plants contain $^{131}I$ in various forms, including molecular iodine ($I_2$), iodide ($I^-$), hypoiodite ion ($IO^-$), and iodate ($IO_3^-$).[3] The long-term exposition (inhaled or swallowed) of radioiodine, even at a low dose, causes severe tissue damage and thyroid cancer. Therefore, it is imperative to capture the aqueous and volatile radioactive iodine in case of a nuclear accident or leak. To contain radioactive iodine, researchers have mainly been developing materials that could adsorb iodine vapor and iodine from organic solvents. To date, the industrial technology to remove radioiodine is based on the chemical transformation of iodine into AgI using silver-doped adsorbents such as natural or synthetic zeolites, $Ag^0$ faujasite or modernite and used as benchmark materials.[4, 5] For decades, a large number of potential adsorbents have been explored to capture iodine from water such as silica-coated magnetite nanoparticles (0.141 g $g^{-1}$),[6] hyperporous carbon (0.926 g $g^{-1}$),[7] and iron oxide nanoparticles@polypyrrole (1.627 g $g^{-1}$).[3] The problems associated with most of these sorbents are their low adsorption capacity, slow adsorption kinetics and inefficient recovery. Over the past years, progress in synthesis chemistry has led to the discovery of promising new porous materials as alternatives to the above-mentioned materials. These porous materials such as metal organic frameworks (MOFs),[8,9,10,11,12] covalent organic frameworks (COFs),[13,14,15,16,17,18] and porous organic polymers (POPs)[8,19] with high and fast adsorption capacity, high specific surface area, high porosity, and good recyclability leads to efficient iodine capture both from vapor and aqueous phase. Recently, a groundbreaking series of studies centered on a group of MOFs derived from UiO-66 was tailored specifically for iodine capture. In their comprehensive exploration, they skillfully incorporated different metals[20,21] ligands[22] and functional groups[23] into the MOF structures, leading to remarkable improvements in iodine capture efficiency. Moreover, the research group also conducted experiments under realistic nuclear accident scenarios, effectively evaluating the performance of UiO-66-$NH_2$ in the presence of gamma irradiation.[24] In 2022, Yu and co-workers reported a classification of the best materials, among which MOF nanosheets able to capture 3.7 g $g^{-1}$ iodine from an aqueous solution reaching.[25] Xie and co-workers reported a COF structure (iCOF-AB-50) with a static $I_2$ uptake capacity of 10.21 g $g^{-1}$ at 75°C.[15] For iodine capture in vapor phase, the best material reported so far is a POP called BisImi-POP@2, that has a maximum capacity of 10.30 g $g^{-1}$.[26] However, as Valizadeh and co-workers rightly point out, the major problem of these porous materials for industrial applications is that they are in form of powder that makes their handling and transportation difficult.[9] In addition they are sensitive to pressure, dust, clogging, mass loss and moisture. Moreover, the regeneration of powders after adsorption relies on energy and time-consuming techniques such as centrifugation and filtration, which hamper their industrial development. Aside from

these issues, MOFs, COFs and POPs are still expensive laboratory materials, mostly synthesized in small amounts. The design of crosslinked polymer networks (CPN) recently emerged as a way to overcome the limitations of powdery materials. CPN are based on the combination of macrocycles and polymers, benefiting from the unique molecular properties of the former and the processability of the latter.[27,28] Macrocycles show excellent performances as platforms in many applications such as molecular recognition,[29] adsorption,[30] catalysis,[31] sensors,[32] and drug delivery.[33] However, the use of macrocycles for water remediation remains drastically hampered by their high cost, the need of purification steps during the synthesis and the low yield of reaction.[34] Recent studies show that promising new material based on macrocycles such as non-porous macrocycles crystal,[35] intrinsically porous materials (IPMs),[36] organic cages[37] and organogels could be prepared.[38] In the literature, several types of synthetic polymer networks based on macrocycles such as crown ethers,[39] cyclodextrine,[40] calixarene,[41,42] cucurbituril[43] and pillararenes[44] have been reported. Recently, Xie et al reported a calix[4]pyrrole-based crosslinked polymer with a high iodine adsorption capacity in both water (3.24 g $g^{-1}$) and vapor (3.38 g $g^{-1}$) phases.[28] As an alternative to these inherent issues, trianglamine represent a prime candidate because it overcomes all these cited issues, this macrocycle can be easily prepared, purified, and scalable at relatively low cost.[36] Furthermore, trianglamine is a macrocycle with guest recognition properties and have been used for several applications such as gas capture/separation,[36] sensors,[45] membranes,[46] and host-guest selectivity.[47,48,49,50] For this purpose, we report for the first time, the synthesis and characterizations of a trianglamine-polymer network. Here, the poly(propylene glycol), tolylene 2,4-diisocyanate namely (PPG) was chosen as the crosslinker and attached to the rim of the trianglamine via the six free secondary amines. Embedding the trianglamine within a crosslinked network overcomes the problems related to handling powdery crystalline materials. Trianglamine powder for radionuclides capture in aqueous media is impractical due to its hydrophobicity and due to the difficulties of handling the powder in case of nuclear waste. In addition, we showed in this work that the proposed trianglamine-polymer networks (Δ@PPG) could be easily and inexpensively fabricated at industrial scales. In this work, we evaluated the adsorption capacities of the two-crosslinked Δ@PPG for iodine capture from vapor phase, water and seawater. In addition, the biocompatibility of Δ@PPG were evaluated in vivo on zebrafish embryos. To the best of our knowledge, no material in the literature has achieved such a high performance in capturing iodine in three different media.

## RESULTS AND DISCUSSION

**Preparation of trianglamine and crosslinked Δ@PPG network.** Trianglamine (Δ) was synthesized following the report by Gawronski and co-workers (Figure S1).[51,52] The obtained Δ powder was fully characterized using 1H and 13C NMR in $CDCl_3$ to confirm the chemical structure (Figure S2-S3). High-resolution mass spectrum (ESI-MS+) and high-resolution elementary analysis were performed and the results are in agreement with the proposed formula suggesting a molecular weight of 649.5 g.$mol^{-1}$ (Figure S4-S5). Thermal gravimetric analysis (TGA) revealed that the trianglamine starts to decompose at 350°C reaching complete degradation at 400°C (Figure S6). Crystallization and melting temperatures of the macrocycle were 45 and 150 °C respectively, as measured by differential scanning calorimetry (DSC) (Figure S7). The purified trianglamine was then crosslinked with difunctional poly(propylene glycol) toluene 2,4-diisocyanate (PPG). The isocyanate functional end-groups were chosen because of their high reactivity towards primary and secondary amines. The reaction between the trianglamine and the difunctional PPG led to the formation of up to six urea functions bridging the macrocycles together and forming a chemically crosslinked network (Scheme 1, Figure S8). The crosslinking density of the network was controlled by varying the ratio between PPG and trianglamine. Two crosslinked networks were thus designed by adding, (a) three equivalents of PPG (denoted Δ@PPG3) and (b) seven equivalents of PPG to ensure grafting of six PPG chains from the six free secondary amines in the structure of the trianglamine (denoted Δ@PPG6). These ratios were chosen to be able to study the influence of the crosslinking density and the amount of trianglamine on the iodine capture. Theoretically, the reaction of three equivalences of PPG should leave three free amine groups and form a weaker crosslinked network (Δ@PPG3, 8.6 w/w % of trianglamine). Using seven equivalences of PPG should lead to the reaction of all the amine groups, forming a highly crosslinked network (Δ@PPG6) containing 4.5 w/w % of trianglamine. The crosslinking efficiency was investigated by calculating the gel content (GC%). As shown in Figure S9, the GC% of the Δ@PPG3 was 87% while for the Δ@PPG6 the value was

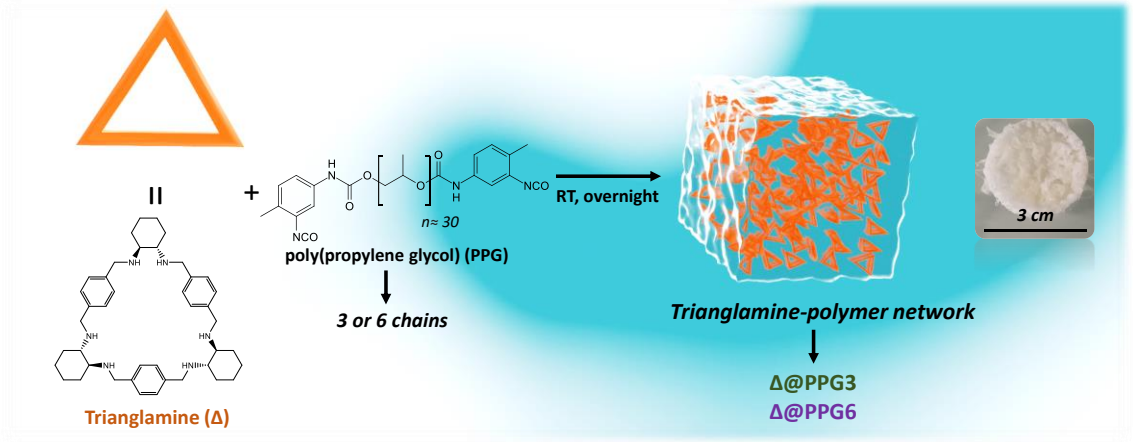


**Scheme 1.** Synthesis of the trianglamine-polymer network (Δ@PPG3 and Δ@PPG6).

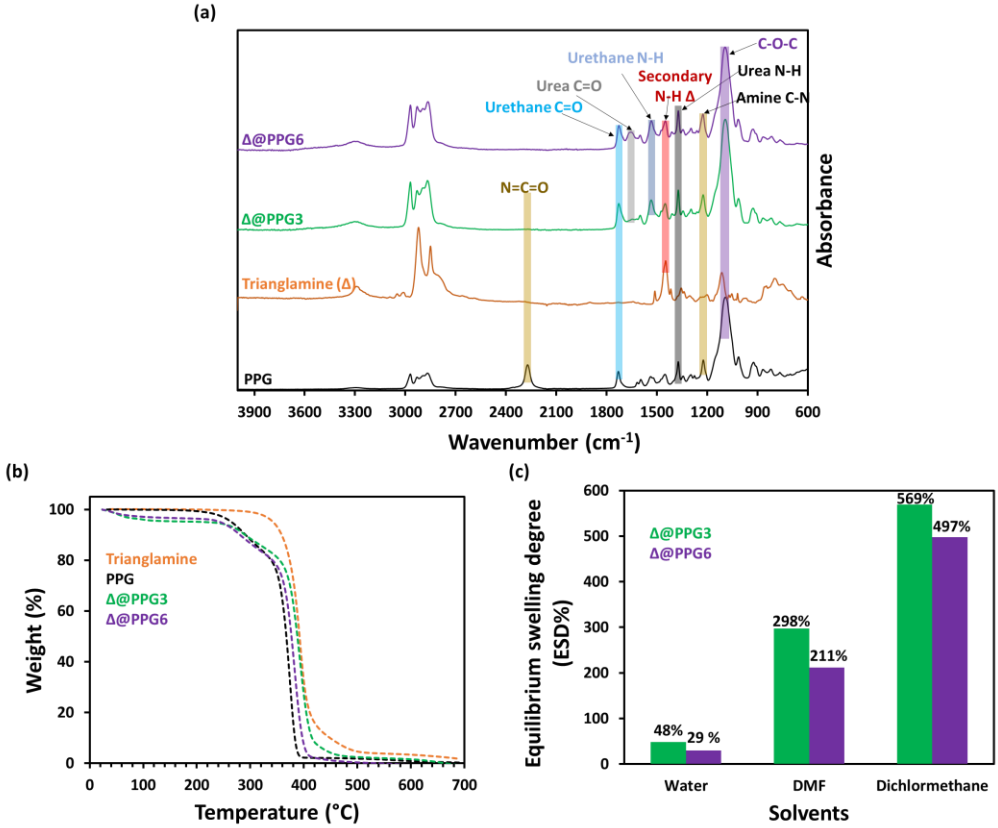


**Figure 1.** (a) FTIR spectra of PPG (black), Δ powder (orange), Δ@PPG3 (green), Δ@PPG6 (purple). (b) TGA of PPG (black), Δ powder (orange), Δ@PPG3 (green), Δ@PPG6 (purple) and (c) equilibrium swelling degree (SD%) of Δ@PPG3 (green), Δ@PPG6 (purple).

96%, suggesting a high degree of crosslinking. The composition and the texture of Δ@PPG3 and Δ@PPG6 were fully characterized using Fourier Transform infrared spectroscopy (FTIR), thermogravimetric analysis (TGA), nitrogen sorption measurements, degree of swelling, Δ@PPG content, and scanning electron microscopy (SEM). The comparison of the FTIR spectra of the reactants PPG and trianglamine with the synthesized trianglamine-polymer networks (Δ@PPG3, Δ@PPG6) are shown in Figure 1a. On the FTIR spectra of the PPG, a stretching vibration band at 2270 $cm^{-1}$ corresponding to the isocyanate N=C=O can be observed. This band disappears after the reaction with the trianglamine. Meanwhile, new signals appeared around 1641 and 1525 $cm^{-1}$ corresponding to the C=O and N-H of the urea function confirming the successful formation of the urea groups and the crosslinked network. Furthermore, the C=O and N-H peaks of the urea bonds are more intense in the Δ@PPG6 network compared to the Δ@PPG3, demonstrating that there are more urea functions and that the crosslinking density is higher in the Δ@PPG6 network. The TGA curves of the trianglamine, the PPG and the resulting networks (Δ@PPG3 and Δ@PPG6) are shown in Figure 3b. The weight losses of the samples were determined by heating the samples to 700 °C under nitrogen at a heating rate of 20 °C $min^{-1}$. In the case of PPG, two weight losses were observed at 210 °C and 310 °C. The trianglamine showed only one weight loss at 320° C. Furthermore, the TGA curves of the Δ@PPG3 and Δ@PPG6 networks were very similar to the PPG, with two weight losses at 260 and 352 °C for Δ@PPG3, and 247 and 342 °C for Δ@PPG6. The temperature of degradation of the Δ@PPG3 is 15°C higher than the Δ@PPG6. This slight difference could be explained by the molar ratio between the trianglamine and PPG (Δ/PPG) in each sample. Increasing the molar ratio of trianglamine results in a more thermally stable crosslinked network as trianglamine degrades at higher temperature as compared to the PPG. The swelling degree (SD%) of the synthesized crosslinked networks were investigated using three different solvents at room temperature: dichloromethane (DCM), dimethylformamide (DMF) and water. The swelling kinetic curves (Figure S10) show that both samples swell in the three tested solvents, and the kinetic of swelling were different from one solvent to another until reaching the equilibrium swelling degree (ESD%). The maximum swelling for both Δ@PPG3 and Δ@PPG6 was reached after 1.5 hours in DCM, 6.5 hours in water and 13.5 hours in DMF. The swelling degree is directly related to the solvent-polymer interactions and the polymer solubility. Solvent-polymer interactions dictate the polymer chain expansion or collapse. In this case, the values of ESD% (Figure 1c) clearly shows that the PPG and the trianglamine that constitute the networks have a better affinity with DCM and DMF thanf water. A less dense network was formed with Δ@PPG3 since solvent could easily penetrate the network, while the dense compact Δ@PPG6 network showed limited solvent penetration hence less swelling. As shown in Figure 1c and Figure S10, the ESD% values of the Δ@PPG3 are higher than those of Δ@PPG6 in the three used solvents; 569% against 497% in the case of DCM, 298% against 211% in case of DMF and 48% against 29% with water. This suggests the formation of two different networks with different crosslinking density. In addition, the stability of the Δ@PPG3 and Δ@PPG6 networks were evaluated in (0.1M) HCl and NaOH. The cross-linked networks showed no signs of degradation over time (monitored over 6 months) (Figure S11). The porosity of the Δ@PPG networks were examined by nitrogen

adsorption and desorption experiments at 77 K. Before the adsorption test, the Δ@PPG samples were degassed for 12 h at 200°C under high vacuum. Only a negligible amounts of nitrogen was adsorbed by the Δ@PPG networks, suggesting that the networks were not porous (no microporosity or mesoporosity were available to adsorb nitrogen) (Figure S12). The Scanning Electron Microscopy (SEM) images show alveolar morphology, which are typical for crosslinked polymer materials (Figure S13).

**Static iodine vapor capture.** First, the capacity of iodine vapor adsorption was evaluated. The vapor adsorption was performed with the crosslinked Δ@PPG6, Δ@PPG3 and the Δ powder under static condition at 77°C and ambient pressure using a vial-in-vial set-up as depicted in Figure S14. The adsorption capacities were determined by weighing the sample before and after iodine exposure at different time intervals. Figure 5a shows the amount of iodine adsorbed over 96 hours. After 48 hours maximum uptake values were reached with 6 g $g^{-1}$ and 5.6 g $g^{-1}$ for Δ@PPG6 and Δ@PPG3 respectively, placing them among the highest-performing adsorbents for static iodine capture reported in the literature (Figure 2a). The obtained data were directly compared with the benchmark adsorbents. The crosslinked Δ@PPG6, Δ@PPG3 have slightly lower uptake than the best reported powder materials (POPs, COFs) but the highest among all the non-powder material such as fibers and beads (Figure 2c and Table S1). Indeed, the crosslinked Δ@PPG6 reached 2-folds higher than the N-MOF-PAN fiber and reached 10-folds higher than the Cu-BTC@PES and HKUST-1@PES beads (Figure 2c). In addition, our crosslinked material performed much better in iodine adsorption compared to all the supramolecular macrocycle-based porous polymers (Table S2). As a comparison, Δ@PPG6 performed 2-folds higher than the reported work by Sessler in 2022 (calix[4]pyrrole-based crosslinked polymer with maximum iodine adsorption of 3.38 g $g^{-1}$).[28] Over the course of iodine vapor exposure, the starting colorless Δ@PPG gradually turned brownish-orange (less than 5 min) before becoming black, confirming the presence of high amounts of iodine and polyiodide trap into the cavity (Figure 2b). The adsorption capacity was decreased after 48 hours probably due to the formation of liquid complexes between $I_2$ and Δ@PPG samples and this phenomenon has been already observed and reported in the literature with the bisimidazole-based conjugated polymers (BisImi-POP2).[15,26].The trianglamine powder was used as the control in the iodine static vapor adsorption. The Δ powder reached a record uptake of ~ 10.53 g $g^{-1}$ much more than

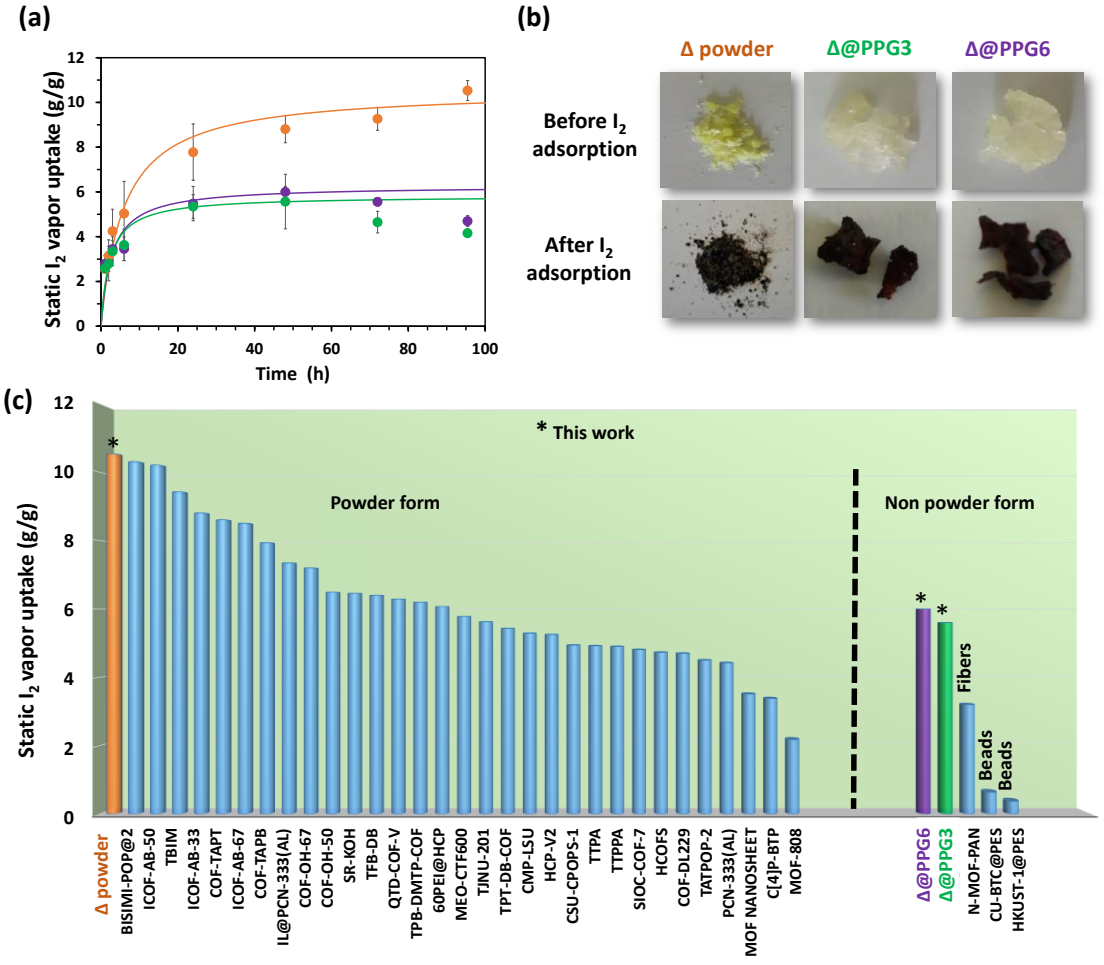


**Figure 2.** Static iodine adsorption performance. (a) Gravimetric measurement of static $I_2$ with Δ powder, Δ@PPG3 and Δ@PPG6, three parallel measurements were achieved for each point. (b) Photographs showing the color change for the trianglamine powder and the polymer networks after exposition to iodine vapor. (c) Comparison of static $I_2$ vapor capture performances of various adsorbents. The orange bar represents the Δ powder, the purple bar the Δ@PPG6, the green bar the Δ@PPG3 and the blue bars correspond to other previously reported adsorbent and references are given in Table S1.

other existing adsorbents (POPs, COFs, MOFs, etc.). To the best of our knowledge, the best iodine capture was reported for a POP (BisImi-POP2) and a COF (iCOF-AB-50) reaching values of 10.30 g $g^{-1}$ and 10.21 g $g^{-1}$, respectively. The high iodine adsorption capacity of the Δ powder could be due to the extraordinary affinity with iodine. The intrinsic cavity of the trianglamine promotes the adsorption of iodine. In order to prove this claim, TGA, FTIR, Raman analysis and optical microscopy of the samples after iodine capture were performed. As expected, TGA presented a weight loss between 60°C and 100°C corresponding to the sublimation of iodine. However, the presence of iodine doesn't affect the thermal stability of the Δ@PPG (Figure S15). FITR spectra showed no red shift between the neat and iodine loaded samples, indicating that the interaction is essentially due to the intrinsic cavity and not from electrostatic interaction with the N sites and aromatic groups of the trianglamine (Figure S16).[13,17] Such results suggest that the adsorption of iodine with the crosslinked Δ@PPG is governed by the physisorption (intrinsic cavity of the trianglamine) and not due to chemisorption. To determine distinct spectroscopy signature for the iodine and polyiodides such as $I_3^-$, $I_5^-$, Δ@PPG@$I_2$ and Δ@$I_2$ samples were analyzed by Raman spectroscopy (Figure S17). Solid iodide displays a Raman peak at 180 $cm^{-1}$, that shifts towards lower frequency when interacting with other material. Therefore, a broad and strong band is observed at 165 – 175 $cm^{-1}$, which is usually attributed to the vibration of adsorbed iodine in a perturbed state due to the interaction with the material.[53] Moreover, the peaks appearing at 111 and 133 $cm^{-1}$ are assigned to the symmetric (ν1) and asymmetric (ν2) stretching frequency of $I_3^-$ anions. To better understand the formation mechanisms of $I_3^-$, several literature studies have provided explanations for the reduction of $I_2 \rightarrow I_3^-$ through the formation of an electron donor-acceptor (EDA) complex between the aromatic ring and iodine molecule.[20,23] Additionally, it has been reported that high electron donor groups, such as -NH, also enhance the adsorption of $I_2$.[21] In our case, even if we do not observe any red shift in infrared after iodine adsorption, there is still a possibility that the secondary amine and the aromatic component from the trianglamine are responsible for the reduction of $I_2$. The optical microscopy images also showed iodine trapped into the Δ powder (Figure S18). To summarize, it could be stated that the presented material are the best for

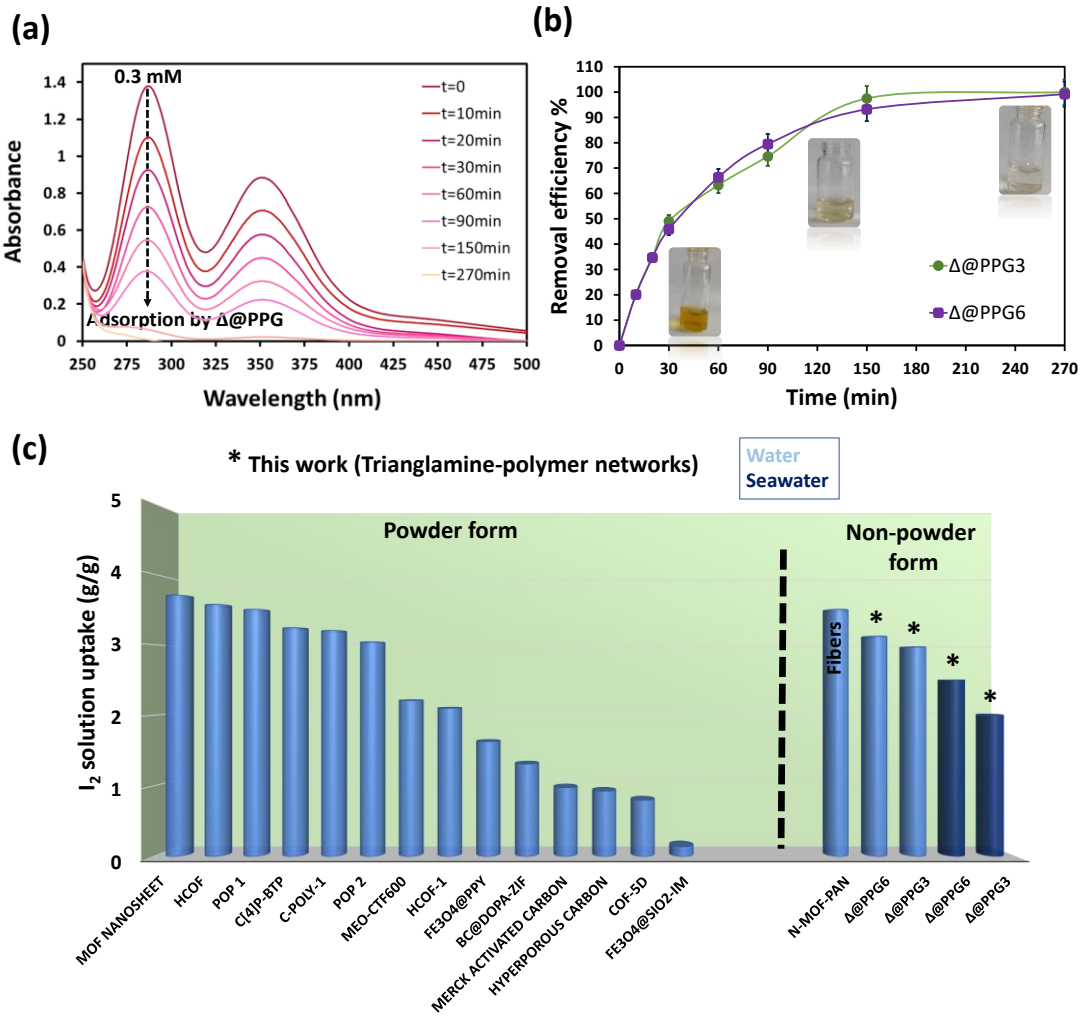


**Figure 3.** (a) UV-Vis spectra of saturated iodine in aqueous solutions before and after adsorption by Δ@PPG3. (b) Time dependent adsorption profiles for the Δ@PPG3 and Δ@PPG6 in iodine aqueous solution of 0.3mM, three parallel measurements were achieved for each point. (c) Comparison of iodine adsorption capacities of various adsorbents, Δ@PPG3 and Δ@PPG6 (water, seawater). The specific $I_2$ solution (water, seawater) capture values of the reported adsorbents and corresponding references are presented in Supplementary Table S4.

iodine adsorption both in the form of powder and non-powder material. When comparing the adsorption values between the neat trianglamine and the trianglamine containing networks, it could be argued that there is no benefit in embedding the trianglamine macrocycles within the polymer network as the iodine capture decreases. However, one should take into account the difficulty of working with powders. The obvious benefit of having the trianglamine within the polymer network is that the handling and regenerating the material would be much easier as well as less energy consuming. In addition, one should take into account the percentage of the trianglamine macrocycles included in the polymer network (8.6 and 4.5 % in Δ@PPG3 and Δ@PPG6 respectively). Taking all these factors in account the results demonstrate that crosslinked polymer networks demonstrate an efficient iodine vapor adsorption. It should also be noted that here, we have evaluated the maximum adsorption capacity of the networks in a closed reactor. However, testing the iodine capture under dynamic adsorption conditions would provide a more industrially valuable data. Given the static data obtained it could be assumed that the synthesized networks would also perform well under dynamic flow conditions.

**Iodine capture from water and seawater.** Radioactive iodine ($^{129}I$ and $^{131}I$) originates from nuclear waste and eventually diffuse into water bodies because of its high volatility and solubility. However, the removal of iodine from water has already been reported,[54,55] although most of the studies have focused on capturing iodine vapor. To the best of our knowledge, not much have been reported on the adsorption of iodine in seawater to mimic real conditions. Generally, iodine tends to form polyiodides in aqueous medium and triiodide ($I_3^-$) is one of the most predominant species.[25,56,57] A theoretical diameter of 5.3 Å for $I_3^-$ was calculated by Zhang et al;[7] in parallel the intrinsic cavity of trianglamine used in our study is 6.3 Å, which can lead the trap of $I_3^-$ through the cavity of the macrocycle.[36] The trianglamine powder was thus used for iodine capture in water and seawater (experimental set-up illustrated in Figure S19). A solution of $I_3^-$ was freshly prepared by diluting a commercial iodine solution at 0.1N to 0.3 mM in deionized water. After addition of the trianglamine powder, the concentration of $I_3^-$ was monitored using UV-visible spectroscopy (Figure S20i). 24h were needed to reach the maximum adsorption value, corresponding to a removal efficiency of 92%. After 4.5h, the removal efficiency was only 48% due to the slow kinetics, probably because of the poor affinity between the hydrophobic trianglamine powder and the aqueous solution providing slow diffusion of iodine species to the macrocycle cavities. Indeed, kinetics data were better fitted with pseudo first order ($R^2$= 0.98) than with pseudo second order ($R^2$=0.88) equations, supporting that the diffusion of species to the active sites is the rate controlling step (Figure S21a, all rate constants, calculated adsorption capacities and correlation coefficient listed in Table S3).[58] In contrast with the trianglamine powder, the crosslinked polymer networks Δ@PPG3 and Δ@PPG6 show fast iodine uptake in water with 92% removal efficiency reached after 2.5h (Figure 3a-b and S20a-d). This enhanced kinetics can be attributed to the polymer networks providing more favorable interactions with water molecules. As a matter of fact, the adsorption curves were correctly fitted with a pseudo second order model ($R^2$=0.98 for Δ@PPG3 and $R^2$=0.9999 for Δ@PPG6, Figure S20c-d, Table S3), suggesting that the diffusion of iodine species to the adsorption sites is not the main rate-limiting step. The role of the PPG polymer network in Δ@PPG was further evidenced by comparison with a pure polymer hydrogel made of poly(ethylene glycol), called PEG hydrogel hereafter, used as a reference to mimic the crosslinked PPG (synthesis protocol described in experimental part). When used as an adsorbent for iodine in aqueous solution, the PEG hydrogel shows an uptake of 53% after 4.5h. In addition, the kinetics data were better fitted with a pseudo second order ($R^2$= 0.99) than with a pseudo first order ($R^2$=0.93) model (Figure S21b, Table S3). These results reveal that: i/ the polymer network is able to adsorb iodine species and ii/ it shows favorable interactions in aqueous media. It thus confirms the beneficial role of the PPG network in Δ@PPG to enhance the adsorption kinetics in water while maintaining a high maximum

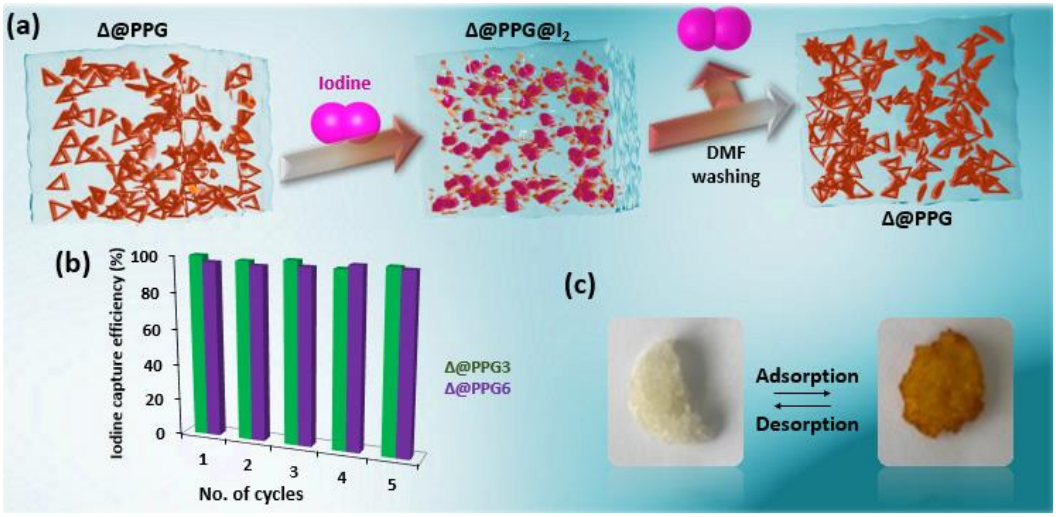


**Figure 4.** (a) Schematic representation of Δ@PPG as the adsorbent for iodine capture and the recycling of Δ@PPG@$I_2$ with DMF. (b) Iodine capture efficiency of Δ@PPG3 and Δ@PPG6 and reversibility tests showing that the adsorption was recycled 5 times with DMF. (c) Photography showing the efficiency of the release of iodine in DMF from the Δ@PPG3@$I_2$ sample.

uptake. Furthermore, Δ@PPG were testes as adsorbents for an iodine solution made with filtrated seawater (seawater from Mediterranean Sea, Palavas les flots-France). A removal efficiency of 80% was reached for both Δ@PPG3 and Δ@PPG6 after 2.5h (Figure S20c and d), which is slightly lower than with deionized water. It probably arises from the high concentration of inorganic salts, organic molecules or microorganisms in the seawater; yet, this result illustrates the capacity of Δ@PPG to adsorb iodine species in a complex authentic media. To determine the maximum iodine uptake capacity in water, adsorption experiments were performed in highly concentrated iodine (0.2 M) solutions. The Δ@PPG samples were immersed in iodine solutions (deionized water and seawater) for 96 hours. The maximum uptake was then calculated using equations 3 and 4. Figure S22 shows the evolution of the discoloration of iodine solutions and the coloration of the Δ@PPG samples over time (18, 24, 48, 72 and 96 hours). The obtained results presented in Figure S23 were compared with the benchmark adsorbents reported in the literature (Figure 3c). Remarkably, Δ@PPG6 and Δ@PPG3 exhibit high uptake capacity in deionized water with 3.12 g $g^{-1}$ and 3 g $g^{-1}$, respectively. Moreover, we report for the first time the use of macrocycle-polymer networks for iodine capture from seawater, with high capacity values of 2.5 g $g^{-1}$ for Δ@PPG6 and 2 g $g^{-1}$ with Δ@PPG3. It was expected that the iodine adsorption would only take place on the surface of the Δ@PPG, since the Δ@PPG had a moderate affinity with water as demonstrated by the swelling experiments (Figure 1c and Figure S10). However, this was not the case as the core of the samples were colored after the absorption experiments indicating that iodine penetrated and diffused all the way inside the samples (Figure S24) despite the moderate affinity with water. It is plausible that both the polymer network and the macrocycle play a role in the iodine capture. Most probably, the iodine gets trapped in the semi-swollen crosslinked PPG network and then gets adsorbed in the intrinsic cavity of the trianglamine. The number of the trianglamine units in the crosslinked networks (4.5 w/w% for Δ@PPG6 and 8.6 w/w% for Δ@PPG3) does not have a considerable effect on the kinetic or the adsorption efficiency. In the context of iodine removal from water and seawater, it should be noted that the hydrophobic nature of trianglamine limits its affinity with aqueous media, thereby decreasing its adsorption performance. However, incorporating the macrocycle within a polymeric matrix, such as polypropylene glycol (PPG), has shown to enhance the materials' affinity with the target media. This incorporation not only improves the adsorption kinetics but also enhances the adsorption capacity of the materials, owing to the synergistic effects of the polymer network.

**Material Recovery/Re-use.** The recovering ability of loaded Δ@PPG3 and Δ@PPG6 were evaluated overnight. DMF was used because it is a good solvent for iodine as well as having a good affinity with Δ@PPG as shown by the swelling studies (Figure 1c and Figure 4a). Both samples (Δ@PPG3 and Δ@PPG6) maintained their high iodine uptake (around 98%) after 5 cycles of washing and loading (Figure 4b, c), confirming an excellent stability and recyclability.

**Filtration of aqueous iodine solution.** The Δ@PPG6 iodine uptake performances were also evaluated in a flow-through setup made of a plastic syringe filled with Δ@PPG6 as depicted in Figure 5a. An aqueous iodine solution (0.3 mM) was passed through the sorbent and the eluent was analyzed. This cycle was repeated twice, resulting in a colorless solution (Figure 5b-c). Figure 5d shows the overlay of the UV-visible spectrum before and after the 1st and the 2nd filtration. After the 1st filtration, the sample adsorbed about 75% of the iodine and 87% after the 2nd filtration. This filtration set up is not optimal, since the packing was not compact and there were gaps between the sample pieces and the syringe wall. This could explain the 25% and 13% residual $I_2$ after the first and second filtrations (Figure S25). The same experiment was performed with a more concentrated iodine solution of 0.2 M (Figure S26). It took six cycles of filtration to reduce significantly the concentration of iodine down as visually shown on Figure S26. Furthermore, the column containing Δ@PPG@$I_2$ could be easily washed and regenerated with DMF.

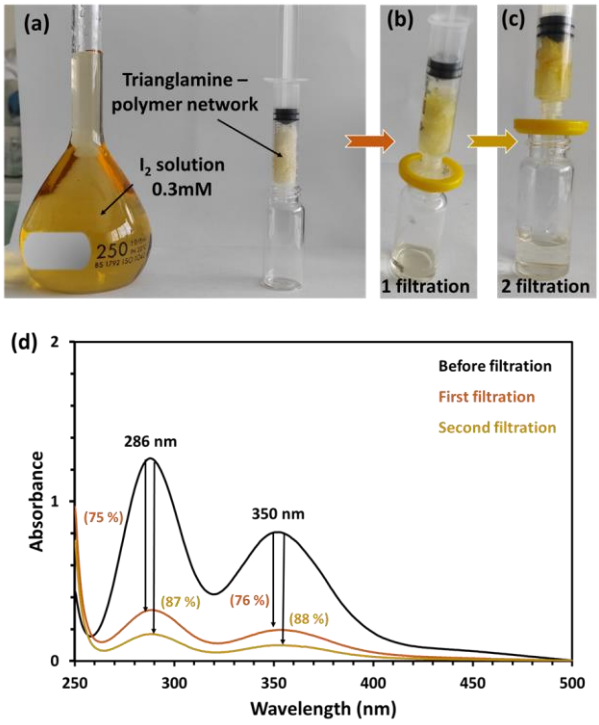


**Figure 5.** (a) Solution of 0.3 mM of iodine and syringe filled with the Δ@PPG6. (b) First filtration of 0.3 mM of aqueous iodine solution through the syringe-Δ@PPG6-filter. (c) Second filtration of mM of aqueous iodine solution. (d) UV-vis spectra of aqueous iodine solution (0.3mM) before and after passing through the syringe set up.

**Biocompatibility Test.** In vivo biocompatibility of Δ@PPG3 and Δ@PPG6 was evaluated on zebrafish embryos. Gastrula stage embryos were maintained in water (4,5 mL / well) added or not with a sample of Δ@PPG3 (36 mg) and Δ@PPG6 (38 mg) (Figure S27). Percentages of chorionated and hatched embryos were analyzed at different hours post fertilization (hpf): 7, 24, 48,72 and 120 hpf (Figure S27-a). Data demonstrated that Δ@PPG3 or Δ@PPG6

didn't induce any toxicity on embryos after 120 hpf of bathing. Indeed, no changes in motility, morphology and hatching rate were observed (Figure S27 - b and c).

## CONCLUSIONS

In summary, we report, for the first time a biocompatible composite crosslinked network made of trianglamine and poly(propylene glycol). The difunctional PPG was reacted with trianglamine at different ratios resulting in formation of crosslinked networks with three or six polymer chains per trianglamine (Δ@PPG3 and Δ@PPG6). Both synthesized samples showed high affinity with iodine regardless of the media (vapor, water, seawater). In vapor phase, ultrahigh uptake capacity of 6 g $g^{-1}$ and 5.6 g $g^{-1}$ were reached for Δ@PPG6 and Δ@PPG3 respectively. The samples also exhibited high iodine adsorption capacity from aqueous media (deionized water and seawater). The highest uptakes were 3.1 g $g^{-1}$ – 2.5 g $g^{-1}$ and 2.9 g $g^{-1}$ – 1.9 g $g^{-1}$, for Δ@PPG6 and Δ@PPG3, respectively. Moreover, kinetics results showed that the polymer network in Δ@PPG allows for a fast uptake of iodine while maintaining a high maximal capacity. In addition, it was demonstrated that these networks are recyclable and retain their uptake capacity after regeneration (tested up to five times of use). As far as we know, the adsorption values obtained for the synthesize Δ@PPG networks are among the highest reported in the three medias tested (vapor phase, deionized water, and seawater). It should also be pointed out that the Δ@PPG networks are simple to make and could easily be prepared at large scale and relatively low cost (as compared to performant material such as COFs and MOFs). Hence, Δ@PPG networks combine excellent adsorption performances, easy handling, simple production, low cost and biocompatible, which demonstrates their safeness and high potential in becoming an attractive industrial product for capturing iodine in nuclear industry.

## MATERIALS AND METHODS

**Materials.** All reagents were purchased from commercial suppliers and used without further purification. (±)-trans-1,2-diaminocyclohexane, terephthalaldehyde, triethylamine, sodium borohydride, Poly(propylene glycol) toluene 2,4-diisocyanate ( Mn~2300 g/mol), poly(ethylene glycol) dimethacrylate polymer (Mn= 700 g/mol), anhydrous chloroform, iodine solution (1.0N), and deuterated solvents were purchased from Sigma Aldrich. The Darocur1173 was purchased from BASF. The seawater was collected from the Mediterranean Sea (South of France, Palavas-les-flots).

**Characterizations**. $^{1}H$ NMR and $^{13}C$ NMR spectrum were recorded on Bruker Avance III 400 MHz. NMR spectrometer in DMSO-d6 and $CDCl_3$. Mass spectrometric analyses were performed in the positive ion mode using a quadrupole mass spectrometer (micromass, Platform II). Mass spectrometric (MS) analyses was performed with SYNAPT G2-S (Waters Corporation, Manchester, UK) equipped with an ESI source. High-resolution electrospray ionization mass spectrometry (HR-ESI-MS) was acquired in positive or negative ion mode. Conditions: capillary voltage 3000 V; cone voltage 20V, dry gas temperature 140 ºC, desolvation temperature = 450°C, dry gas flow, 1000 $L.h^{-1}$ and nitrogen as nebulizer gas, Pressure = 6.5 bars. 1ng/µl Leucine Enkephalin was used as standard for internal calibration. UV-Visible spectrometry measurements were conducted in a 1 cm PMMA cuvette using a UV–vis spectrophotometer (UV-2401PC, Shimadzu, Kyoto, Japan). FTIR (Fourier transform infrared spectroscopy) analysis were monitored on a Thermo Nicolet Nexus FTIR spectrometer with a diamond ATR attachment, samples were subjected to 32 scans in the range of 4000 $cm^{-1}$ and 650 $cm^{-1}$. Thermogravimetric analysis (TGA) was measured by TA Instruments SDT Q600 by heating the sample to 700 °C under nitrogen (60 mL $min^{-1}$) at a heating rate of 20 °C $min^{-1}$. Raman spectroscopy measurements were conducted using a Renishaw in Via Raman microscope equipped with an x10 objective (Leica) under illumination of 532 nm laser. The grating used was standard 1800 l/mm grating with 1 $cm^{-1}$ spectral resolution, to study the materials thoroughly the non-destructive way of sample measurement was opted. The LASER power user for the measurements was 0.05% of the peak power 4mW i.e. 0.002mW. We calculate the power density if the LASER by P/A where p is power and A is area of the LASER. The area of the LASER can be calculated by beam diameter multiplied by the magnification used during the measurements.

$A=26 \times 10=260\ mm^2$

$P=0.002\ mW \div 260\ mm^2$

$P=0.0000769\ W/cm^2$

The fluence (F) can be calculated by:

$F = E/A$

E= p(power) × t (exposure time))/Area)

$F= (0.002\ mW \times 40000\ mS) \div 260\ mm^2= 0.003077\ Jouls/cm^2$

**Synthesis of the Δ.** A mixture of (±)-trans-1,2-diaminocyclohexane (2.28 g, 20 mmol), terephthalaldehyde (2.68g, 20 mmol) was added in methanol solution (200 mL) with triethylamine (7.0 mL, 50 mmol) and stirred overnight. The mixture was cooled in an ice bath and sodium borohydride (2.28 g, 60 mmol) was added over one hour to reduce trianglimine in trianglamine. After a stirring of three hours at room temperature, the solvents were removed under vacuum and the residue was dissolved in dichloromethane (100 ml) and washed with aqueous sodium carbonate (5%) and water. The organic extract was dried with magnesium sulfate and then evaporated and dried under vacuum at 50°C during five hours. Trianglamine was obtained in a yield of 4 g (90%). In order to obtain pure trianglamine, the macrocycle was solubilized with 4 mL of absolute EtOH. A solution of 10 mL of absolute EtOH with 2 mL of concentrated HCl (37%) was added dropwise to the absolute trianglamine mixture. The formation of white precipitate was observed during the addition. The solid was filtered and dried under vacuum. The white solid was dissolved in water and make it basic with (20 mL, 2 M NaOH) solution, which form a white precipitate during the addition. The pure precipitate trianglamine (Δ) was filtered and dried under vacuum desiccator for one day at 50 °C.

**Preparation of trianglamine-polymer networks.** Two different crosslinking rates were prepared as follow: In a first vial, 100 mg of trianglamine (Δ) was dissolved in 0.5mL of dichloromethane. In a second vial, 3eq or 6eq of poly (pro-

pylene glycol) 2,4-diisocyanate (Mn~2300 g/mol) was dissolved in 1 mL of dichloromethane. Both vials were covered and placed in ice-bath for 30 min, in order to slow down the reactivity of isocyanate groups. The trianglamine solution was quickly added to PPG solution, agitated by hand, and closed. In less than 1 minute the Δ@PPG is formed and left for 24 hours to be sure that all isocyanate has been reacted. In the end, the Δ@PPG were washed, by swelling in dichloromethane to remove the unreacted reagents (PPG and trianglamine (Δ)); the solvent was exchanged every 12 hours for 3 days. Then, the Δ@PPG of trianglamine-polymer networks were dried under reduced pressure.

FTIR: 3294 $cm^{-1}$ (m; νs(NH), 3000-2800 $cm^{-1}$ (s; νs (NH) and (m; νs(CH)), 1725 $cm^{-1}$ (s; νs(C=O), 1606 $cm^{-1}$ (s; νs(C=O), 1517 $cm^{-1}$ (m; νb(NH), 1442 $cm^{-1}$ (m; νb(NH)), 1369 $cm^{-1}$ (m; νb(NH)), 1212 $cm^{-1}$ (m; νs(C-N)), 1078 $cm^{-1}$(s; νs(C-O).

**Preparation of poly(ethylene glycol) hydrogel (PEG Hydrogel).** 500 mg of poly(ethylene glycol) dimethacrylate polymer (Mn= 700 g/mol) and 10 mg of Darocur 1173 photoinitiator were dissolved in 1 mL of water and then successfully photo crosslinked in a UV chamber at 365 nm during 10 min. The obtained hydrogel was washed by immersing in water during 2 days and the water was changed 3 times.

**Network studies.** *Gel content* (GC%) of Δ@PPG: After the fabrication step, the Δ@PPG were first dried to constant weight (W0) and purified by immersing in dichloromethane (DCM) for 24 hours. After this step, Δ@PPG were dried again to record the final weight (Wext). The Δ@PPG fraction (GC%) was calculated according to Equation 1:

$$GC\% = (W_{ext}/W_0)\times 100 \quad (1)$$

*Swelling degree (SD%) and equilibrium swelling degree (ESD%) measurement* the swelling behavior of the Δ@PPG was determined by placing a weighed dry polymer network (Wx) into deionized water, dimethylformamide (DMF) or dichloromethane (DCM) at room temperature (25 °C). The swollen Δ@PPGs were removed from the solvents bath at specific time intervals, wiped superficially with filter paper, weighed (Wy) and sunk back into the corresponding solvents. The measurements were carried out until the weight of the swollen Δ@PPG reached a constant value corresponding to the equilibrium swelling degree (ESD). The experiments were done three times, and the average value measurements were reported. The swelling degree at various time intervals, expressed as amount of solvent absorbed by the dry Δ@PPG, was calculated using Equation (2). The ESD% was determined as the value corresponding to the curve plateau of the swelling degree (SD%).

$$SD\% = ((Wy-Wx)/Wx)*100 \quad (2)$$

Where Wx is the weight of the Δ@PPG (before swelling), and Wy is the weight of the swollen Δ@PPG at different times t (hours).

**Iodine capture in vapor phase.** The iodine vapor adsorption capacities of Δ@PPGs were calculated by mass measurements. 100 mg of each A= Δ@PPG3, B= Δ@PPG6, and C= trianglamine powder, were introduced into vessels, which contained an amount of solid $I_2$. Then the vessel was then sealed and heated using an oven at 77°C for 0.5−96 h to allow the adsorption of iodine by samples. The iodine-loaded samples were cooled to room temperature and the iodine uptake was evaluated by gravimetry at different times. The iodine capture of Δ@PPGs was evaluated by the following equation $(W_2 - W_1)/W_1$. Where $W_1$ and $W_2$ represent the mass of Δ@PPGs before and after iodine capture, respectively.

**Iodine capture in aqueous phase.** Adsorption in water and seawater in order to monitor the $I_2$ capture speed of Δ@PPGs in an aqueous solution (water or Mediterranean seawater), a time-dependent UV-Vis measurement was carried out on a UV-Vis spectrophotometer. Δ@PPG (100 mg) were added to an $I_2$ aqueous solution (V= 50 mL, C= 0.3mM). The UV-Vis spectrum of the solution was recorded every 10 minutes in the first 30 mins, and at 1 h, 1h30, 2h30, and 4h30, respectively. The $I_2$ concentration at different intervals was calculated using a calibration curve.

**Desorption and recyclability of Δ@PPG.** The adsorption/desorption experiment: was monitored as follow; 100 mg of Δ@PPGs was introduced in an aqueous iodine solution (C= 0.3 mM, V= 50mL), the UV-visible was taken after 4.5h. Then the iodine-loaded Δ@PPGs were immersed in 50 mL of DMF for 24h in order to desorb the iodine. The experiment of uptake and release of iodine was repeated several 5 times in order to monitor the efficiency of adsorption/desorption cycles.

**Maximum iodine uptake in water and seawater.** 200 mg of each (Δ@PPG3 and Δ@PPG6) were placed in a highly concentrated iodine solution (C= 0.2M, V= 20 mL), in order to determine the maximum uptake of iodine, that the polymer networks can uptake. After 96h, the mother solution (0.2M) was diluted to reach the concentration of 0.3mM, and the final solution at T= 96h was equally diluted, to be analyzed by UV-visible spectroscopy. The final concentration and the weight of captured iodine were determined using a UV calibration curve and the following equations:

$$W_i = (A.V.M)/K \quad \ldots\ldots\ldots\ldots\ldots (3)$$

$$\text{Maximum uptake (g/g)} = W_i/W_{\Delta@PPG} \quad \ldots\ldots\ldots\ldots\ldots (4)$$

Where:

$W_i$= weight of iodine, A= UV absorbance, V= volume of iodine solution, M = molecular weight of I2, K= constant of Beer Lamber law, $W_{\Delta@PPG}$= masse of Δ@PPG in gram.

*The adsorption experiment in seawater was performed the same way as in deionized water.

**Filtration process.** In a 12 ml plastic syringe, the Δ@PPG Δ@PPG6 (1.2 g) was pushed and stacked in the bottom of the syringe plastic. The syringe was equipped with 0.22 µm PVDF syringe filter with a diameter of 30 mm. The aqueous iodine solution at 0.3 mmol. $L^{-1}$ was passed one time through the Δ@PPG with a flow rate of ~1 mL/min. Then, the filtrate was recovered and passed again through the same syringe with the same flow rate. The UV-vis spectra were recorded before and after the first and the second filtrations.

***In vivo* toxicity in zebrafish embryos.** Wild-type AB zebrafish strain was purchased from Zebrafish International Resource Center (ZIRC) as embryos and were raised to adulthood in circulating aquarium system inside environmentally controlled room (28 °C, 80% humidity, 14 h light/10 h dark cycle), in the lab's facilities of Molecular mechanisms in neurodegenerative dementia (MMDN), Inserm U1198, Montpellier University, Montpellier. Fertilized

embryos were collected and maintained at 28 °C. At 7 hours post fertilization (hpf), embryos were examined under the microscope, and only embryos that developed normally and reached gastrula stage were selected for the study. Selected embryos were placed in 12 well plate (6 embryos per well) and exposed to 4.5 mL water containing or not samples of trianglamine polymer networks Δ@PPG3 (36 mg) and Δ@PPG6 (38 mg). The percentages of survival, malformation, mortality and hatching embryos were recorded with Olympus MVX10 macroview microscope at 7, 24, 48, 72 and 120 hpf. Experiments with zebrafish embryos until 120 hpf are considered as in vitro studies according to the EU Directive 2010/63/EU on the protection of animals used for scientific purposes.

## ASSOCIATED CONTENT

### Supporting Information

The Supporting Information is available free of charge on the ACS Publications website.

1H and 13C NMR spectra for all compounds, MS spectra, elemental analysis, TGA, DSC, Swelling degree, BET, SEM, FTIR, Raman, UV analysis, reaction schemes, additional bio-experimental details, and photographs of experimental setup and samples.

## AUTHOR INFORMATION


### Corresponding Author

**Mona Semsarilar** - *Institut Européen des Membranes, IEM, Univ Montpellier, CNRS, ENSCM, Montpellier, France. Email: Mona.semsarilar@umontpellier.fr*

**Arnaud Chaix** - *Institut Européen des Membranes, IEM, Univ Montpellier, CNRS, ENSCM, Montpellier, France. Email: arnaud.chaix@umontpellier.fr*

### Author

**Belkacem Tarek Benkhaled** - *Institut Européen des Membranes, IEM, Univ Montpellier, CNRS, ENSCM, Montpellier, France.*

**Chaimaa Gomri** - *Institut Européen des Membranes, IEM, Univ Montpellier, CNRS, ENSCM, Montpellier, France.*

**Sébastien Buys** - *Institut Européen des Membranes, IEM, Univ Montpellier, CNRS, ENSCM, Montpellier, France.*

**Nabil Namar** - *Institut Européen des Membranes, IEM, Univ Montpellier, CNRS, ENSCM, Montpellier, France.*

**Nadine Sehoulia** - *Institut Européen des Membranes, IEM, Univ Montpellier, CNRS, ENSCM, Montpellier, France.*

**Rohitkumar Jadhav** - *Institut Européen des Membranes, IEM, Univ Montpellier, CNRS, ENSCM, Montpellier, France.*

**Jason Richard** - *Institut Européen des Membranes, IEM, Univ Montpellier, CNRS, ENSCM, Montpellier, France.*

**Laure Lichon** - *IBMM, Univ Montpellier, CNRS, ENSCM, Montpellier, France.*

**Christophe Nguyen** - *IBMM, Univ Montpellier, CNRS, ENSCM, Montpellier, France.*

**Magali Gary-Bobo** - *IBMM, Univ Montpellier, CNRS, ENSCM, Montpellier, France.*


### Author Contributions

‡ B. T. B. and A. C. contributed equally.

### Notes

The authors declare no competing financial interest.

## ACKNOWLEDGMENT


The authors would like to thank the French National Research Agency (ANR) and MUSE (University of Montpellier) for funding this work under contracts PEPPISA-19-CE06-0011-01 and ERC-IMOPS. This work was also supported by the Laboratoire d'Excellence sur la Chimie des Systèmes Moléculaires et Interfaciaux (LabEx CheMISyst). We thank zebrafish platform of the laboratory: Molecular mechanisms in neurodegenerative dementia (MMDN), Inserm U1198.


## REFERENCES


(1) Intenational Energy Agency (IEA), Nuclear Power in a Clean Energy System, IEA Paris https://www.iea.org/reports/nuclear-power-in-a-clean-energy-system, May 2019, License: CC BY 4.0.

(2) Huve, J.; Ryzhikov, A.; Nouali, H.; Lalia, V.; Augé, G.; Daou, T. J. Porous Sorbents for the Capture of Radioactive Iodine Compounds: A Review. *RSC Adv.* **2018**, *8* (51), 29248–29273.

(3) Harijan, D. K. L.; Chandra, V.; Yoon, T.; Kim, K. S. Radioactive Iodine Capture and Storage from Water Using Magnetite Nanoparticles Encapsulated in Polypyrrole. *J. Hazard. Mater.* **2018**, *344*, 576–584.

(4) Sava Gallis, D. F.; Ermanoski, I.; Greathouse, J. A.; Chapman, K. W.; Nenoff, T. M. Iodine Gas Adsorption in Nanoporous Materials: A Combined Experiment-Modeling Study. *Ind. Eng. Chem. Res.* **2017**, *56* (8), 2331–2338.

(5) DePaoli, D. W.; Nan, Y.; Tavlarides, L. L. Adsorption of Iodine on Hydrogen-reduced Silver-exchanged Mordenite Experiments and Modeling. *AIChE Journal*. **2017**, *63*, 1024-1035.

(6) Madrakian, T.; Afkhami, A.; Zolfigol, M. A.; Ahmadi, M.; Koukabi, N. Application of Modified Silica Coated Magnetite Nanoparticles for Removal of Iodine from Water Samples. *Nano-Micro Lett.* **2012**, *4* (1), 57–63.

(7) Zhang, Q. M.; Zhai, T. L.; Wang, Z.; Cheng, G.; Ma, H.; Zhang, Q. P.; Zhao, Y. H.; Tan, B.; Zhang, C. Hyperporous Carbon from Triptycene-Based Hypercrosslinked Polymer for Iodine Capture. *Adv. Mater. Interfaces* **2019**, *6* (9). 1900249.

(8) Xie, W.; Cui, D.; Zhang, S. R.; Xu, Y. H.; Jiang, D. L. Iodine Capture in Porous Organic Polymers and Metal-Organic Frameworks Materials. *Materials Horizons*. **2019**, *6*, 1571–1595.

(9) Valizadeh, B.; Nguyen, T. N.; Smit, B.; Stylianou, K. C. Porous Metal–Organic Framework@Polymer Beads for Iodine Capture and Recovery Using a Gas-Sparged Column. *Adv. Funct. Mater.* **2018**, *28* (30), 1801596.

(10) Tang, Y.; Huang, H.; Li, J.; Xue, W.; Zhong, C. IL-Induced Formation of Dynamic Complex Iodide Anions in IL@MOF Composites for Efficient Iodine Capture. *J. Mater. Chem. A* **2019**, *7* (31), 18324–18329.

(11) Chen, P.; He, X.; Pang, M.; Dong, X.; Zhao, S.; Zhang, W. Iodine Capture Using Zr-Based Metal-Organic Frameworks (Zr-MOFs): Adsorption Performance and Mechanism. *ACS Appl. Mater. Interfaces* **2020**, *12* (18), 20429–20439.

(12) Sava, D. F.; Rodriguez, M. A.; Chapman, K. W.; Chupas, P. J.; Greathouse, J. A.; Crozier, P. S.; Nenoff, T. M. Capture of Volatile Iodine, a Gaseous Fission Product, by Zeolitic Imidazolate Framework-8. *J. Am. Chem. Soc.* **2011**, *133* (32), 12398–12401.

(13) Xie, Y.; Pan, T.; Lei, Q.; Chen, C.; Dong, X.; Yuan, Y.; Maksoud, W. Al; Zhao, L.; Cavallo, L.; Pinnau, I.; Han, Y. Efficient and Simultaneous Capture of Iodine and Methyl Iodide Achieved by

a Covalent Organic Framework. *Nat. Commun.* **2022**, *13* (1), 1–10.

(14) Lin, Y.; Jiang, X.; Kim, S. T.; Alahakoon, S. B.; Hou, X.; Zhang, Z.; Thompson, C. M.; Smaldone, R. A.; Ke, C. An Elastic Hydrogen-Bonded Cross-Linked Organic Framework for Effective Iodine Capture in Water. *J. Am. Chem. Soc.* **2017**, *139* (21), 7172–7175.

(15) Xie, Y.; Pan, T.; Lei, Q.; Chen, C.; Dong, X.; Yuan, Y.; Shen, J.; Cai, Y.; Zhou, C.; Pinnau, I.; Han, Y. Ionic Functionalization of Multivariate Covalent Organic Frameworks to Achieve an Exceptionally High Iodine-Capture Capacity. *Angew. Chemie - Int. Ed.* **2021**, *60* (41), 22432–22440.

(16) Wang, P.; Xu, Q.; Li, Z.; Jiang, W.; Jiang, Q.; Jiang, D. Exceptional Iodine Capture in 2D Covalent Organic Frameworks. *Adv. Mater.* **2018**, *30* (29), 1801991.

(17) Liu, C.; Jin, Y.; Yu, Z.; Gong, L.; Wang, H.; Yu, B.; Zhang, W.; Jiang, J. Transformation of Porous Organic Cages and Covalent Organic Frameworks with Efficient Iodine Vapor Capture Performance. *J. Am. Chem. Soc.* **2022**, *144* (27), 12390–12399.

(18) Liao, Y.; Li, J.; Thomas, A. General Route to High Surface Area Covalent Organic Frameworks and Their Metal Oxide Composites as Magnetically Recoverable Adsorbents and for Energy Storage. *ACS Macro Lett.* **2017**, *6* (12), 1444–1450.

(19) Das, M.; Sarkar, S. K.; Patra, Y. S.; Manna, A.; Mukherjee, S.; Das, S. Soft Self-Templating Approach-Derived Covalent Triazine Framework with Bimodal Nanoporosity for Efficient Radioactive Iodine Capture for Safe Nuclear Energy. *ACS Appl. Nano Mater.* **2022**, *5* (7), 8783–8793.

(20) Andrade, P. H. M.; Henry, N.; Volkringer, C.; Loiseau, T.; Vezin, H.; Hureau, M.; Moissette, A. Iodine Uptake by Zr-/Hf-Based UiO-66 Materials: The Influence of Metal Substitution on Iodine Evolution. *ACS Appl. Mater. Interfaces* **2022**, *14* (26), 29916–29933.

(21) Andrade, P. H. M.; Moreau, M.; Henry, N.; Bakouche, M. T.; Duval, S.; Volkringer, C.; Loiseau, T.; Hureau, M.; Moissette, A. Raman Mapping as a Tool for Evaluating I2 and I3– Diffusion Over Single-Crystal UiO-67_NH2(M) (M = Zr, Zr/Hf, or Hf). *J. Phys. Chem. C* **2023**, *127* (9), 4618–4635.

(22) Leloire, M.; Walshe, C.; Devaux, P.; Giovine, R.; Duval, S.; Bousquet, T.; Chibani, S.; Paul, J.-F.; Moissette, A.; Vezin, H.; Nerisson, P.; Cantrel, L.; Volkringer, C.; Loiseau, T. Capture of Gaseous Iodine in Isoreticular Zirconium-Based UiO-n Metal-Organic Frameworks: Influence of Amino Functionalization, DFT Calculations, Raman and EPR Spectroscopic Investigation. *Chem. – A Eur. J.* **2022**, *28* (14), e202104437.

(23) Abramova, A.; Couzon, N.; Leloire, M.; Nerisson, P.; Cantrel, L.; Royer, S.; Loiseau, T.; Volkringer, C.; Dhainaut, J. Extrusion-Spheronization of UiO-66 and UiO-66_NH2 into Robust-Shaped Solids and Their Use for Gaseous Molecular Iodine, Xenon, and Krypton Adsorption. *ACS Appl. Mater. Interfaces* **2022**, *14* (8), 10669–10680.

(24) Leloire, M.; Dhainaut, J.; Devaux, P.; Leroy, O.; Desjonqueres, H.; Poirier, S.; Nerisson, P.; Cantrel, L.; Royer, S.; Loiseau, T.; Volkringer, C. Stability and Radioactive Gaseous Iodine-131 Retention Capacity of Binderless UiO-66-NH2 Granules under Severe Nuclear Accidental Conditions. *J. Hazard. Mater.* **2021**, *416*, 125890.

(25) Yu, C. X.; Li, X. J.; Zong, J. S.; You, D. J.; Liang, A. P.; Zhou, Y. L.; Li, X. Q.; Liu, L. L. Fabrication of Protonated Two-Dimensional Metal-Organic Framework Nanosheets for Highly Efficient Iodine Capture from Water. *Inorg. Chem.* **2022**, *61* (35), 13883–13892.

(26) Niu, T.; Feng, C.; Yao, C.; Yang, W.; Xu, Y. Bisimidazole-Based Conjugated Polymers for Excellent Iodine Capture. **2020**, 3, 354-361.

(27) Lim, J. Y. C.; Goh, S. S.; Liow, S. S.; Xue, K.; Loh, X. J. Molecular Gel Sorbent Materials for Environmental Remediation and Wastewater Treatment. *J. Mater. Chem. A* **2019**, *7* (32), 18759–18791.

(28) Xie, L.; Zheng, Z.; Lin, Q.; Zhou, H.; Ji, X.; Sessler, J. L.; Wang, H. Calix[4]Pyrrole-Based Crosslinked Polymer Networks for Highly Effective Iodine Adsorption from Water. *Angew. Chemie - Int. Ed.* **2022**, *61* (1).

(29) Barrow, S. J.; Kasera, S.; Rowland, M. J.; Del Barrio, J.; Scherman, O. A. Cucurbituril-Based Molecular Recognition. *Chemical Reviews*. **2015**, *115*, 12320–12406.

(30) Wu, H.; Jones, L. O.; Wang, Y.; Shen, D.; Liu, Z.; Zhang, L.; Cai, K.; Jiao, Y.; Stern, C. L.; Schatz, G. C.; Stoddart, J. F. High-Efficiency Gold Recovery Using Cucurbit[6]Uril. *ACS Appl. Mater. Interfaces* **2020**, *12* (34), 38768–38777.

(31) Li, Z.; Yang, Y. W. Macrocycle-Based Porous Organic Polymers for Separation, Sensing, and Catalysis. *Advanced Materials*. **2022**, *34*, 2107401.

(32) Pinalli, R.; Pedrini, A.; Dalcanale, E. Biochemical Sensing with Macrocyclic Receptors. *Chem. Soc. Rev.* **2018**, *47* (18), 7006–7026.

(33) Webber, M. J.; Langer, R. Drug Delivery by Supramolecular Design. *Chemical Society Reviews*. Royal Society of Chemistry **2017**, *46*, 6600–6620.

(34) Skorjanc, T.; Shetty, D.; Trabolsi, A. Pollutant Removal with Organic Macrocycle-Based Covalent Organic Polymers and Frameworks. *Chem*. Elsevier Inc. **2021**, *7*, 882–918.

(35) Jie, K.; Zhou, Y.; Li, E.; Li, Z.; Zhao, R.; Huang, F. Reversible Iodine Capture by Nonporous Pillar[6]Arene Crystals. *J. Am. Chem. Soc.* **2017**, *139*, 15320-15323.

(36) Chaix, A.; Mouchaham, G.; Shkurenko, A.; Hoang, P.; Moosa, B.; Bhatt, P. M.; Adil, K.; Salama, K. N.; Eddaoudi, M.; Khashab, N. M. Trianglamine-Based Supramolecular Organic Framework with Permanent Intrinsic Porosity and Tunable Selectivity. *J. Am. Chem. Soc.* **2018**, *140* (44), 14571–14575.

(37) Percástegui, E. G.; Jancik, V. Coordination-Driven Assemblies Based on Meso-Substituted Porphyrins: Metal-Organic Cages and a New Type of Meso-Metallaporphyrin Macrocycles. *Coord. Chem. Rev.* **2020**, *407*, 213165.

(38) Li, B.; Wang, B.; Huang, X.; Dai, L.; Cui, L.; Li, J.; Jia, X.; Li, C. Terphen[n]Arenes and Quaterphen[n]Arenes (N=3–6): One-Pot Synthesis, Self-Assembly into Supramolecular Gels, and Iodine Capture. *Angew. Chemie - Int. Ed.* **2019**, *58* (12), 3885–3889.

(39) Ge, Z.; Hu, J.; Huang, F.; Liu, S. Responsive Supramolecular Gels Constructed by Crown Ether Based Molecular Recognition. *Angew. Chemie* **2009**, *121* (10), 1830–1834.

(40) Liao, X.; Chen, G.; Liu, X.; Chen, W.; Chen, F.; Jiang, M. Photoresponsive Pseudopolyrotaxane Hydrogels Based on Competition of Host-Guest Interactions. *Angew. Chemie - Int. Ed.* **2010**, *49* (26), 4409–4413.

(41) Lee, J. H.; Park, J.; Park, J. W.; Ahn, H. J.; Jaworski, J.; Jung, J. H. Supramolecular Gels with High Strength by Tuning of Calix[4]Arene-Derived Networks. *Nat. Commun.* **2015**, *6*, 1–9.

(42) Zhang, J.; Guo, D. S.; Wang, L. H.; Wang, Z.; Liu, Y. Supramolecular Binary Hydrogels from Calixarenes and Amino Acids and Their Entrapment-Release of Model Dye Molecules. *Soft Matter* **2011**, *7* (5), 1756–1762.

(43) Appel, E. A.; Biedermann, F.; Rauwald, U.; Jones, S. T.; Zayed, J. M.; Scherman, O. A. Supramolecular Cross-Linked Networks via Host-Guest Complexation with Cucurbit[8]Uril. *J. Am. Chem. Soc.* **2010**, *132* (40), 14251–14260.

(44) Li, Y. F.; Li, Z.; Lin, Q.; Yang, Y. W. Functional Supramolecular Gels Based on Pillar[: N] Arene Macrocycles. *Nanoscale*. **2020**, *12*, 2180–2200.

(45) Chappanda, K. N.; Chaix, A.; Surya, S. G.; Moosa, B. A.; Khashab, N. M.; Salama, K. N. Trianglamine Hydrochloride Crystals for a Highly Sensitive and Selective Humidity Sensor. *Sensors Actuators, B Chem.* **2019**, 294, 40-47.

(46) Huang, T.; Moosa, B. A.; Hoang, P.; Liu, J.; Chisca, S.; Zhang, G.; AlYami, M.; Khashab, N. M.; Nunes, S. P. Molecularly-Porous Ultrathin Membranes for Highly Selective Organic Solvent Nanofiltration. *Nat. Commun.* **2020**, *11* (1), 1–10.

(47) Liu, X.; Alimi, L. O.; Khashab, N. M. Highly Selective Molecular Sieving of Cis- over Trans-1,2-Dichloroethene Isomers. *Chem. Commun.* **2022**, *58* (67), 9369–9372.

(48) Ding, Y.; Alimi, L. O.; Du, J.; Hua, B.; Dey, A.; Yu, P.; Khashab, N. M. Pillar[3]Trianglamines: Deeper Cavity Triangular Macrocycles for Selective Hexene Isomer Separation†. *Chem. Sci.* **2022**, *13* (11), 3244–3248.

(49) Dey, A.; Chand, S.; Ghosh, M.; Altamimy, M.; Maity, B.; Bhatt, P. M.; Bhat, I. A.; Cavallo, L.; Eddaoudi, M.; Khashab, N. M. Molecular Recognition and Adsorptive Separation Ofm-Xylene by Trianglimine Crystals. *Chem. Commun.* **2021**, 57, 9124-9127.

(50) Dey, A.; Chand, S.; Maity, B.; Bhatt, P. M.; Ghosh, M.; Cavallo,

L.; Eddaoudi, M.; Khashab, N. M. Adsorptive Molecular Sieving of Styrene over Ethylbenzene by Trianglimine Crystals. *J. Am. Chem. Soc.* **2021**, *143*, 4090-4094.

(51) Gawroński, J.; Kołbon, H.; Kwit, M.; Katrusiak, A. Designing Large Triangular Chiral Macrocycles: Efficient [3 + 3] Diamine-Dialdehyde Condensations Based on Conformational Bias. *J. Org. Chem.* **2000**, *65* (18), 5768–5773.

(52) Gawronski, J.; Gawronska, K.; Grajewski, J.; Kwit, M.; Plutecka, A.; Rychlewska, U. Trianglamines - Readily Prepared, Conformationally Flexible Inclusion-Forming Chiral Hexamines. *Chem. - A Eur. J.* **2006**, *12* (6), 1807–1817.

(53) Spadoni, A.; Falconieri, M.; Lanchi, M.; Liberatore, R.; Marrocco, M.; Sau, G. S.; Tarquini, P. Iodine Compounds Speciation in HI-I2 Aqueous Solutions by Raman Spectroscopy. *Int. J. Hydrogen Energy* **2012**, *37* (2), 1326–1334.

(54) Zhao, X.; Han, X.; Li, Z.; Huang, H.; Liu, D.; Zhong, C. Enhanced Removal of Iodide from Water Induced by a Metal-Incorporated Porous Metal–Organic Framework. *Appl. Surf. Sci.* **2015**, *351*, 760–764.

(55) Liu, Y.-J.; Sun, Y.-F.; Shen, S.-H.; Wang, S.-T.; Liu, Z.-H.; Fang, W.-H.; Wright, D. S.; Zhang, J. Water-Stable Porous Al24 Archimedean Solids for Removal of Trace Iodine. *Nat. Commun.* **2022**, *13* (1), 6632.

(56) Svensson, P. H.; Kloo, L. Synthesis, Structure, and Bonding in Polyiodide and Metal Iodide-Iodine Systems. *Chem. Rev.* **2003**, *103* (5), 1649–1684.

(57) Huang, M.; Yang, L.; Li, X.; Chang, G. An Indole-Derived Porous Organic Polymer for the Efficient Visual Colorimetric Capture of Iodine in Aqueous Media: Via the Synergistic Effects of Cation-π and Electrostatic Forces. *Chem. Commun.* **2020**, *56* (9), 1401–1404.

(58) Wang, J.; Guo, X. Adsorption Kinetic Models: Physical Meanings, Applications, and Solving Methods. *J. Hazard. Mater.* **2020**, *390*, 122156.

# TOC

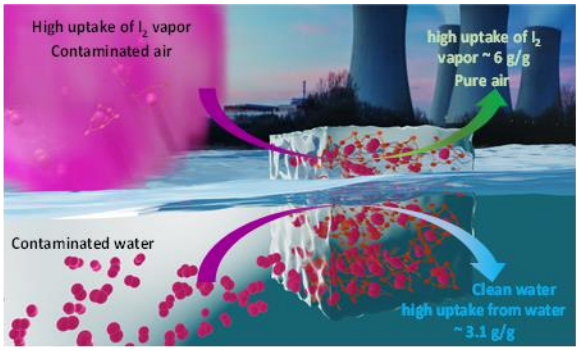
High uptake of $I_2$ vapor
Contaminated air
high uptake of $I_2$ vapor ~ 6 g/g
Pure air
Contaminated water
Clean water
high uptake from water
~ 3.1 g/g